Journal of Nanofluids
Vol. 10, pp. 431–446, 2021
(www.aspbs.com/jon)

ARTICLE

Ion Slip and Hall Effects on Generalized Time-Dependent Hydromagnetic Couette Flow of Immiscible Micropolar and Dusty Micropolar Fluids with Heat Transfer and Dissipation: A Numerical Study

Rajesh Kumar Chandrawat[1,*], Varun Joshi[1], and O. Anwar Bég[2]

[1]*Department of Mathematics, Lovely Professional University Jalandhar, 144411, India*
[2]*Professor and Director-Metaphysical Engineering Sciences Group (MPESG), Department Mechanical/Aeronautical Engineering, School of Science, Engineering, Environment (SEE), Salford University, Manchester, M54WT, UK*

The hydrodynamics of immiscible micropolar fluids are important in a variety of engineering problems, including biofluid dynamics of arterial blood flows, pharmacodynamics, Principle of Boundary layers, lubrication technology, short waves for heat-conducting fluids, sediment transportation, magnetohydrodynamics, multicomponent hydrodynamics, and electrohydrodynamic. Motivated by the development of biological fluid modeling and medical diagnosis instrumentation, this article examines the collective impacts of ion slip, viscous dissipation, Joule heating, and Hall current on unsteady generalized magnetohydrodynamic (MHD) Couette flow of two immiscible fluids. Two non-Newtonian incompressible magnetohydrodynamic micropolar and micropolar dusty (fluid-particle suspension) fluids are considered in a horizontal duct with heat transfer. No-slip boundary conditions are assumed at the channel walls and constant pressure gradient. Continuous shear stress and fluid velocity are considered across the interface between the two immiscible fluids. The coupled partial differential equations are formulated for fluids and particle phases and the velocities, temperatures, and microrotation profiles are obtained. Under the physically realistic boundary and interfacial conditions, the Modified cubic-B-spline differential quadrature approach (MCB-DQM) is deployed to obtain numerical results. The influence of the magnetic, thermal, and other pertinent parameters, i.e. Hartmann magnetic number, Eckert (dissipation) number, Reynolds number, Prandtl number, micropolar material parameters, Hall and ion-slip parameters, particle concentration parameter, viscosity ratio, density ratio, and time on velocity, microrotation, and temperature characteristics are illustrated through graphs. The MCB-DQM is found to be in good agreement with accuracy and the skin friction coefficient and Nusselt number are also explored. It is found that fluids and particle velocities are reduced with increasing Hartmann numbers whereas they are elevated with increment in ion-slip and Hall parameters. Temperatures are generally enhanced with increasing Eckert number and viscosity ratio. The simulations are relevant to nuclear heat transfer control, MHD energy generators, and electromagnetic multiphase systems in chemical engineering.

KEYWORDS: Micropolar Fluid, Immiscible Fluid, Unsteady Flow, Modified Cubic B-Spline, Differential Quadrature Method, Magnetohydrodynamics.

1. INTRODUCTION

Micropolar fluid dynamics has emerged as a significant branch of modern non-Newtonian fluid mechanics and has been deployed successfully in an impressive range of applications including hemodynamics, geothermic, pharmacodynamics, turbulent shear flows, sensors, liquid crystals, and lubrication systems. Micropolar liquids are non-Newtonian liquids comprising of rigid non-deformable particles which can spin i.e. possess gyratory degrees of freedom. The properties of non-Newtonian fluids cannot be sufficiently described by the Navier-Stokes equations. Eringen developed the fundamental model of

*Author to whom correspondence should be addressed.
Email: rajesh.16786@lpu.co.in
Received: 25 April 2021
Accepted: 30 May 2021

micropolar fluids[1] as a simplification of his earlier theory of micro-morphic fluids ("simple microfluids"). Kang and Eringen[2] applied the micropolar model to blood flow demonstrating its superiority to many other rheological models. Micropolar fluids with heat transfer were investigated by Fakour et al.[3] The interaction between non-deformable spheroids rotating through a micropolar fluid was analyzed using a collocation scheme by Sherief et al.[4] Saad et al.[5] derived the thermophoretic velocity and torque for semi-infinite micropolar fluid with Fourier thermal conductivities. Mehryan et al.[6] investigated natural convection inside a porous embedded channel filled with micropolar nanofluid. Under the MHD effect, heat transfer and flow with variable viscosity inside a duct containing micropolar fluid have been investigated by Javed and Siddiqui.[7] Tetbirt et al.[8] presented a numerical investigation of magnetohydrodynamic flow of micropolar and viscous fluids in a vertical duct.

The integration of micro-sized crystals (dust particles) in hybrid nanofluids is commonly used to improve the thermal conductivity of the base fluid, also known as dusty fluid. It has a variety of implementations, covering combustion, crude oil filtration, and electrostatic precipitation. Menni et al.[9] provides a comprehensive analysis of the computational and experimental studies conducted by numerous scholars to improve convection in porous environments with nanofluids. Reddy et al.[10] identified the heat and mass transportations for micropolar dusty boundary layer flow. The intrinsic configuration of the channel for thermal and kinetic study with Newtonian and turbulent fluid has been extensively examined by Menni et al.[11] and the integration of dynamic objects into solar channels has been investigated.

Micropolar dusty fluids are increasingly being used in engineering applications such as polymeric processing, metal spinning, synovial lubrication, artificial fabrics, cardio-vascular flows, glass-fiber processing, paper production, peristaltic transfer, drug distribution, emulsion suspensions, and colloidal fluids. The analysis of hybrid nanoparticle suspension in micropolar fluids has been assessed comprehensively by Ghadikolaei et al.[12–14] Kaneez et al.[15] exhibits the major aspect of microstructured and dust particles in viscoelastic micropolar fluid with heat energy transportation. Nabwey et al.[16] extensively studied the transient MHD boundary layer flow micropolar hybrid nanofluid. Ahmad et al.[17] investigated the micropolar fluid with dust and hybrid nanoparticles suspension and enhanced the heat transfer effect. The analysis of nanotube suspension in MHD micropolar dusty fluid has been reported by *Eid* et al.[18] Makinde et al.[19] described a numerical analysis for MHD melting micropolar fluid in heat control processing systems. Menni et al.[20] provided a systematic analysis of the different heat transfer techniques utilized to increase the efficiency of the smoother air duct.

Immiscible flows arise in nuclear engineering power systems, the pharmaceutical industry, as well as in the extraction and purification of crude oil in petroleum engineering. These applications have stimulated interest in mathematical modeling and some studies on the flow of immiscible transport phenomena have been communicated. Devakar et al.,[21,22] determined the effect of various fluid parameters featuring only in one immiscible fluid and also the resulting velocity and temperature distributions in the other immiscible fluid. Srinivas et al.[23–25] explored the dynamics of dual immiscible fluid flows in various configurations and with multiple thermodynamics, magnetic and time-dependent effects. There is little more research on the movement of immiscible fluids between two plates for Newtonian and non-Newtonian fluids can be seen Umavathi et al.[26–28]

The theory of the magnetic characteristics and nature of electromagnetic conducting fluids are applicable in various scientific fields such as plasma confinement, molten metals, power generation, drug targeting, and microfluidics. Because of its relevance and uses in different areas such as magnetic drug monitoring astronautics, and astrophysics, researchers are studying magnetohydrodynamic flows at a rapid pace around the world. Attia et al.[29,30] did an extensive study of various magneto-thermodynamics flow parameters on dusty fluids. MHD micropolar fluid flow and heat distribution in channels were addressed by Ashraf et al.[31] The impact of applied transversely uniform magnetic field unsteady MHD. The effect of externally transverse applied uniform magnetic field on unsteady MHD flow has been discovered by Krishna et al.[32] Krishna[33] investigated the thermal and magnetic factors on unsteady rotating MHD flow of Jeffery fluid. In the presence of electromagnetic energy, the analytical solutions of an unsteady -MHD Boussinesq fluid including heat and mass transport properties are proposed Krishna et al.[34] across a vertical undulating plate enclosed in a Darcian permeable medium

The power-law stream with heat transfer and the magnetohydrodynamic impact was examined by Prasad et al.[35] Devakar et al.[36] presented the unsteady MHD flow of immiscible micropolar and Newtonian fluids inside the parallel plate and found the effect of numerous fluid parameters on flow velocity and temperature profile. Some more remarkable studies on Ion slip and Hall effect on MHD flow can be seen in Refs. [37–40].

To analyzing a system of partial differential equations, many computational approaches are available. Menni et al.[41] performed a numerical analysis of heat transfer for fluid flow using flat rectangular and V-upstream geometries. A numerical simulation for unsteady-MHD flow was carried by Krishna et al.[42] using the B-spline collocation method. The effects of specific baffle forms on the radiant aerodynamic efficiency were investigated by Menni et al.[43] using turbulent forced-convection fluid flow models. Some more fascinating fluid flow simulations with different shapes and geometry can be seen in Refs. [44–47].

The differential quadrature method (DQM) is known as one of the most prominent methods for dealing with unsteadiness and nonlinear terms in the coupled partial differential equation. Joshi et al.[48] solved the nonlinear Burgers equation for higher dimensions. Katta et al.[49] solved the time-dependent flow of Jeffery fluid between two porous plates using the trigonometric B-spline differential quadrature method. Two immiscible micropolar and Newtonian fluids were considered in the horizontal channel and the system of partial differential equations was solved by the modified cubic B-Spline differential quadrature method.[50]

Researchers have presented multiple studies on the steady and unsteady flow of single and immiscible combination of micropolar, Newtonian fluids via different shapes and numerical simulation resulting in a variety of effects. To the best of the authors' awareness, no effort has yet been made to investigate the unsteady flow of two immiscible magnetohydrodynamic micropolar and micropolar dusty (fluid-particle suspension) fluids. In light of this, the current study investigates theoretically and computationally the composite effects of ion slip, viscous dissipation, Joule heating, and Hall current effect on unsteady *generalized* Couette flow of two immiscible non-Newtonian incompressible magnetohydrodynamic micropolar and micropolar dusty (fluid-particle suspension) fluids through a horizontal channel. *The novelty is embodied in the simultaneous inclusion of multiple magnetic effects, a sophisticated micromorphic non-Newtonian model, and an alternative computational algorithm (modified cubic B-Spline differential quadrature method) which has never been considered collectively in previous studies.* Ionslip and Hall's current effects have been extensively studied by Bég and co-workers[51–54] in the context of nuclear reactor transport modeling and magnetohydrodynamic energy generators (MHD). These studies have confirmed the substantial modification in velocity and temperature distributions produced with Hall current and ion slip which are relevant to, for example, seeded potassium interfacial flows in Hall and Faraday generator systems[55–58] and also hydromagnetic pumps and channel flow control in nuclear reactors.[59,60] In the present study, the inclusion of such effects is therefore justified. The mathematical model is formulated as a system of coupled partial differential equations and suitable transformations are implemented to render the boundary value problem as non-dimensional. Robust numerical results are obtained for velocity, microrotation, and temperature profiles under the effect of various important fluid parameters. Detailed interpretation is included.

2. MATHEMATICAL FORMULATION

The following assumptions are made for time-dependent, generalized Couette flow of two immiscible, micropolar and micropolar dusty fluids through a horizontal duct (channel).

- Both fluids are electrically conducting, incompressible, unidirectional, and occupied in a horizontal channel comprised of two parallel upper and lower plates as depicted in Figure 1.
- The walls of the channel are separated by a distance of $2k$. The lower wall is fixed and situated at $y = -k$, with constant temperature T_{w1} while the upper wall moves with constant velocity U_0 at $y = k$, has a temperature T_{w2}.
- The flow is induced by the upper plate movement and a constant pressure gradient $(-(\partial p/\partial x))$ which is applied in the x-direction of the channel
- Both walls of the duct are electrically non-conductive and are located in the X–Z plane and both fluids are assumed to have electrical conductivity, σ.

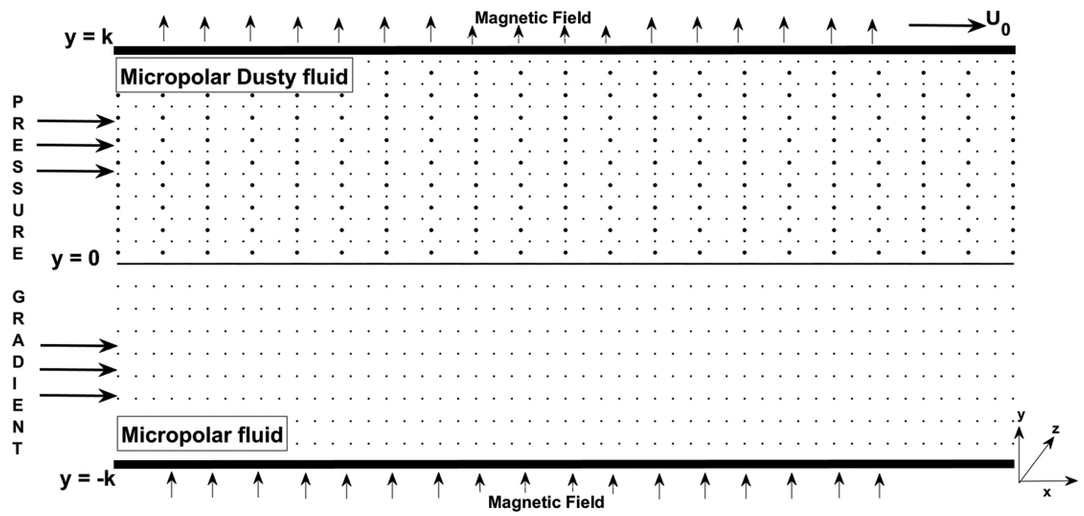

Fig. 1. Geometric configuration of problem.

ARTICLE

ARTICLE

• An external uniform static magnetic field B_0 is imposed on the fluids in the y-direction.
• The effect of an applied transverse magnetic field on both fluids generates resistance to fluid movement through the Lorentz force which is orthogonal to the applied magnetic field and produces the following body force acting on both fluids:[29]

$$J \times B_0 = \frac{\sigma {B_0}^2 (1 + Bi.Be)\, u_i}{(1 + Bi.Be)^2 + Be^2} \tag{1}$$

where J is current density, B_0 is the external magnetic field, σ is the electric conductivity, Bi is the ion slip parameter, Be is the Hall parameter.
• As the fluids are immiscible, the micropolar fluid occupies the lower region of the channel i. e. *zone I* ($-k \le y \le 0$), and possesses a linear fluid velocity u_1, microrotation (angular velocity) M_1, density ρ_1, viscosity μ_1, vortex viscosity κ_1, gyro-viscosities γ_1 and β_1, gyration parameter j_1, thermal conductivity K_1, specific heat capacity C_{P1}.
• Micropolar dusty fluid occupies the upper region of the channel i. e. *zone II* ($0 \le y \le k$) and possesses *linear* fluid velocity u_2, microrotation (angular velocity) M_2 density ρ_2, viscosity μ_2, vortex viscosity κ_2, gyro-viscosities γ_2 and β_2, gyration parameter j_2, thermal conductivity K_2 and specific heat capacity C_{P2}.
• The micropolar dusty (upper region) fluid contains suspended dust particles that have the same size and mass, are non-deformable, and are homogeneously distributed throughout the fluid.
• In the dusty fluid, the dust particles have particle velocity u_p, density ρ_p, and possess the average mass m_p with a particle volume fraction function $\varnothing$.
• It is also assumed that the particle phase is sufficiently dilute such that the interactions between any two particles are ignored, and the dust particle size *(radius r)* is also relatively tiny in scale. Hence the *net dust effect on the fluid particles* is equivalent to the following additional force per unit volume:[12, 29]

$$D_f = KN\left(u_2 - u_p\right) \tag{2}$$

Here $K = 6\pi r \mu_2 U_0$ is the Stokes drag coefficient, N is the density number of a dust particle, μ_2 is the viscosity of upper region fluid.
• Dust particles acquire heat from the fluid by thermal conduction through their surface. Designating c_p as for the specific heat capacity of the particles, the heat conduction *between* the fluid and particles depends on the temperature relaxation parameter γ_T which adopting the approach in Refs. [12, 29] may be stated as.

$$\gamma_T = \frac{3}{2}\frac{\rho_p.c_p.\mu_2}{K.N.K_2} \tag{3}$$

• Body forces and body couples are neglected. The transportation attributes are unchanged in both the zones and common pressure gradients are applied along the horizontal (X) axial direction.
• The following convention is adopted-fluid velocity vectors $u_i = u_i(y, t)$, micro-rotation vector $M_i = M_i(y, t)$, temperature vector $T_i = T_i(y, t)$ in both zones ($i = 1, 2$) and particle velocity $u_p(y, t)$ in zone II (upper).
• The fluid layers are mechanically coupled through the mode of momentum exchange. Transferring momentum arises through consistency in velocity and shear stress *over the interface*. However, we assume that the flow rate and shear pressure are also stable at the interface between two liquids.
• The governing equations for linear fluid velocities (u_1, u_2) particle velocity (u_p), micro-rotation (M_1, M_2) and temperature (T_1, T_2) particle temperature (T_p) of the interfacial MHD (magnetohydrodynamic) flow under the aforesaid assumed constraints are:[12, 29, 36]

Zone-I (Micropolar fluid: $-k \le y \le 0$).

$$\rho_1 \frac{\partial u_1}{\partial t} = -\frac{\partial p}{\partial x} + \kappa_1 \frac{\partial M_1}{\partial y} + (\mu_1 + \kappa_1)\frac{\partial^2 u_1}{\partial y^2} - \frac{\sigma {B_0}^2 (1 + Bi.Be)}{(1 + Bi.Be)^2 + Be^2} u_1 \tag{4}$$

$$\rho_1 j_1 \frac{\partial M_1}{\partial t} = \gamma_1 \frac{\partial^2 M_1}{\partial y^2} - \kappa_1 (2M_1 + \frac{\partial u_1}{\partial y}) \tag{5}$$

$$\rho_1 C_{P1} \frac{\partial T_1}{\partial t} = K_1 \frac{\partial^2 T_1}{\partial y^2} + \mu_1 \left(\frac{\partial u_1}{\partial y}\right)^2 + \kappa_1 \left(2M_1 + \frac{\partial u_1}{\partial y}\right)^2 + \beta_1 \left(\frac{\partial M_1}{\partial y}\right)^2 + \frac{\sigma {B_0}^2 (1 + Bi.Be)}{(1 + Bi.Be)^2 + Be^2} {u_1}^2 \tag{6}$$

Zone-II (Micropolar dusty fluid: $0 \le y \le k$)

$$\rho_2 \frac{\partial u_2}{\partial t} = -\frac{\partial p}{\partial x} + \kappa_2 \frac{\partial M_2}{\partial y} + (\mu_2 + \kappa_2)\frac{\partial^2 u_2}{\partial y^2} - \frac{\sigma {B_0}^2 (1 + Bi.Be)}{(1 + Bi.Be)^2 + Be^2} u_2 - KN\varnothing \frac{(u_2 - u_p)}{(1 - \varnothing)} \tag{7}$$

$$m_p \frac{\partial u_p}{\partial t} = KN\left(u_2 - u_p\right) \tag{8}$$

$$\rho_2 j_2 \frac{\partial M_2}{\partial t} = \gamma_2 \frac{\partial^2 M_2}{\partial y^2} - \kappa_2 (2M_2 + \frac{\partial u_2}{\partial y}) \tag{9}$$

$$\rho_2 C_{P2} \frac{\partial T_2}{\partial t} = K_2 \frac{\partial^2 T_2}{\partial y^2} + \mu_2 \left(\frac{\partial u_2}{\partial y}\right)^2 + \kappa_2 \left(2M_2 + \frac{\partial u_2}{\partial y}\right)^2 + \beta_2 \left(\frac{\partial M_2}{\partial y}\right)^2 + \frac{\sigma {B_0}^2 (1 + Bi.Be)}{(1 + Bi.Be)^2 + Be^2} {u_2}^2 + \frac{\rho_p c_p \varnothing \left(T_p - T_2\right)}{\gamma_T (1 - \varnothing)} + KN\rho_p \varnothing \frac{\left(u_2 - u_p\right)^2}{(1 - \varnothing)} \tag{10}$$

$$\frac{\partial T_p}{\partial t} = -\frac{\left(T_p - T_2\right)}{\gamma_T} \tag{11}$$

At the channel wall, both velocity and microrotation are prescribed the vanishing classical hyper-stick and no-slip conditions at the boundaries are considered. Furthermore, velocities, microrotations, temperature vectors, shear

stress, and couple stress are continuous at the fluid-fluid interface. Both fluids and boundaries (channel walls) are initially sustained at a constant temperature. The temperatures on both walls are set to T_{w1} and T_{w2}, respectively. The initial and boundary conditions are taken as:[12, 29, 36]

Initial conditions: At

$$t \le 0, \quad u_1(y,t) = M_1(y,t) = 0, \quad T_1(y,t) = T_0, \quad \text{for} \quad -k \le y \le 0 \tag{12}$$

$$u_2(y,t) = u_p(y,t) = M_2(y,t) = 0,$$
$$T_2(y,t) = T_p(y,t) = T_0 \quad \text{for} \quad 0 \le y \le k \tag{13}$$

Boundary and interface conditions: At

$$t > 0, \quad u_1(-k,t) = 0, \quad M_1(-k,t) = 0,$$
$$T_1(-k,t) = T_{w1}, \quad u_2(k,t) = U_0,$$
$$u_p(k,t) = U_0, \quad M_2(k,t) = 0,$$
$$T_2(k,t) = T_{w2}, \quad T_p(k,t) = T_{w2} \tag{14}$$

At

$$y = 0, \quad u_1(0,t) = u_2(0,t), \quad M_1(0,t) = M_2(0,t),$$
$$T_1(0,t) = T_2(0,t), \quad \text{and} \quad K_1 T_{1_y} = K_2 T_{2_y}$$
$$(\mu_1 + \kappa_1) U_{1_y} + \kappa_1 M_1 = (\mu_2 + \kappa_2) U_{2_y} + \kappa_2 M_2 \tag{15}$$

The following non-dimensional parameters are introduced:

$$\overline{x} = \frac{x}{k}, \quad \overline{y} = \frac{y}{k}, \quad \overline{u_1} = \frac{u_1}{U_0}, \quad \overline{u_2} = \frac{u_2}{U_0}, \quad \overline{U_p} = \frac{u_p}{U_0},$$
$$\overline{p} = \frac{p}{\rho_1 {U_0}^2}, \quad \overline{t} = \frac{tU_0}{k}, \quad \overline{T_1} = \frac{T_1 - T_{w1}}{T_{w2} - T_{w1}},$$
$$\overline{T_2} = \frac{T_2 - T_{w2}}{T_{w2} - T_{w1}}, \quad \overline{T_p} = \frac{T_p - T_{w2}}{T_{w2} - T_{w1}}, \quad \overline{M_1} = \frac{M_1 k}{U_0},$$
$$\overline{M_2} = \frac{M_2 k}{U_0} \tag{16}$$

Here following[27] we assume $\gamma_1 = (\mu_1 + \kappa_1/2) j_1$ and $\gamma_2 = (\mu_2 + \kappa_2/2) j_2$ with $j_1 = j_2 = k^2$. After dropping the bars, the Eqs. (3)–(9) assume the following forms:

Zone-I (Micropolar fluid: $-k \le y \le 0$).

$$\frac{\partial u_1}{\partial t} = -\frac{\partial p}{\partial x} + \frac{1}{Re}\left[\eta_1 \frac{\partial M_1}{\partial y} + (1+\eta_1)\frac{\partial^2 u_1}{\partial y^2} - \frac{Ha^2(1+Bi.Be)}{(1+Bi.Be)^2 + Be^2} u_1\right] \tag{17}$$

$$\frac{\partial M_1}{\partial t} = \frac{1}{Re}\left[\left(1+\frac{\eta_1}{2}\right)\frac{\partial^2 M_1}{\partial y^2} - \eta_1\left(2M_1 + \frac{\partial u_1}{\partial y}\right)\right] \tag{18}$$

$$\frac{\partial T_1}{\partial t} = \frac{Ec}{Re}\left[\frac{1}{Pr.Ec}\frac{\partial^2 T_1}{\partial y^2} + \left(\frac{\partial u_1}{\partial y}\right)^2 + \eta_1\left(2M_1 + \frac{\partial u_1}{\partial y}\right)^2 + \delta_1\left(\frac{\partial M_1}{\partial y}\right)^2 + \frac{Ha^2(1+Bi.Be)}{(1+Bi.Be)^2 + Be^2} {u_1}^2\right] \tag{19}$$

Zone-II (Micropolar dusty fluid: $0 \le y \le k$)

$$\frac{\partial u_2}{\partial t} = -\frac{\partial p}{\partial x} + \frac{r_1}{r_2.Re}\left[\eta_2 \frac{\partial M_2}{\partial y} + (1+\eta_2)\frac{\partial^2 u_2}{\partial y^2} - \frac{Ha^2(1+Bi.Be)}{r_1\left((1+Bi.Be)^2 + Be^2\right)} u_2 - R\left(u_2 - u_p\right)\right] \tag{20}$$

$$\frac{\partial u_p}{\partial t} = \frac{R.r_1.r_3}{r_2.Re}\left(u_2 - u_p\right) \tag{21}$$

$$\frac{\partial M_2}{\partial t} = \frac{r_1}{r_2.Re}\left[\left(1+\frac{\eta_2}{2}\right)\frac{\partial^2 M_2}{\partial y^2} - \eta_2\left(2M_2 + \frac{\partial u_2}{\partial y}\right)\right] \tag{22}$$

$$\frac{\partial T_2}{\partial t} = \frac{Ec.r_1}{Re.r_2.C_r}\left[\frac{Kr}{Pr.Ec.r_1}\frac{\partial^2 T_2}{\partial y^2} + \left(\frac{\partial u_2}{\partial y}\right)^2 + \eta_2\left(2M_2 + \frac{\partial u_2}{\partial y}\right)^2 + \delta_2\left(\frac{\partial M_2}{\partial y}\right)^2 + \frac{Ha^2(1+Bi.Be)}{r_1\left((1+Bi.Be)^2 + Be^2\right)} {u_2}^2 + \frac{2}{3}\frac{R.K_r}{Pr.Ec.r_1} \times \left(T_p - T_2\right) + \frac{R.C_r.r_3}{Ec}\left(U_2 - U_p\right)^2\right] \tag{23}$$

$$\frac{\partial T_p}{\partial t} = \frac{2}{3}\frac{R * k_r * C_r * r_3}{C_{Pr} * r_1 * Pr}\frac{\left(T_2 - T_p\right)}{Re} \tag{24}$$

Eqs. (12)–(15) are considered as *initial, interfacial, and boundary conditions* with $T_0 = 0$, $T_{w1} = 0$, $T_{w2} = 1$, $U_0 = 1$, and $k = 1$. In Eqs. (17)–(24) the parameters (see nomenclature) emerging are defined as follows: $Re = (\rho_1 U_0)/\mu_1$, $\eta_1 = (\kappa_1/\mu_1)$, $Ha^2 = (\sigma {B_0}^2 k^2)/\mu_1$, $Ec = (U_0/C_{P1})(T_{w2} - T_{w1})$, $Pr = (\mu_1 C_{P1})/K_1$, $\delta_1 = (\beta_1/\mu_1 k^2)$, $r_1 = (\mu_2/\mu_1)$, $r_2 = (\rho_2/\rho_1)$, $\eta_2 = (\kappa_2/\mu_2)$, $R = (KNk^2\varnothing)/(\mu_2(1-\varnothing))$, $r_3 = (\rho_2/\rho_p)$, $C_r = (C_{P2}/C_{P1})$, $\delta_2 = \beta_1/(\mu_1 k^2)$, $K_r = (K_2/K_1)$, $C_{Pr} = (C_{P2}/c_p)$ and $-(\partial p/\partial x) = Ge(t)$ is the applied time-dependent pressure gradient in the x-axial direction with $t > 0$.

3. NUMERICAL SOLUTION

To compute the fluid velocity and temperature distribution for *schemes I and II*, the interval $[-1, 1]$ is divided as $[-1, 0]$ for the non-dusty micropolar fluid and $[0, 1]$ for dusty micropolar fluid. Next both domains are likewise discretized with step size h in the y-(transverse) axis and k' in the time.

$$a = y_1 < y_2 < \ldots < y < y_n = b,$$
$$\text{such that } y_{i+1} - y_i = h \text{ on the real axis.} \tag{25}$$

Following this, let $R_{i_y}(y_i, t)$ denote the first and $R_{i_{yy}}(y_i, t)$ denote the second-order derivatives of

$u_1(y,t), u_2(y,t), u_P(y,t), T_1(y,t), T_2(y,t)$, and $T_P(y,t)$ which are obtained at any time on the nodes x_i:

$$\text{For } i=1,2,3,\ldots,n. \quad R_{1y}(y_i,t)=\sum_{j=1}^{N} a^*_{ij} R_i(y_j,t), \quad \text{for } j=1,2,\ldots,N$$

$$R_{1yy}(y_i,t)=\sum_{j=1}^{N} b^*_{ij} R_i(y_j,t), \text{ for } j=1,2,\ldots,N \quad (26)$$

Here a^*_{ij} b^*_{ij} are the weight-coefficients of the first and second-order derivative of each associated with the y-coordinate which are quantified using the cubic B-spline function. The cubic B-spline of the knots are as specified below:

$$\vartheta_j=\frac{1}{h^3}\begin{cases}(y-y_{j-2})^3, & y\epsilon[y_{j-2},y_{j-1})\\ (y-y_{j-2})^3-4(y-y_{j-1})^3, & y\epsilon[y_{j-1},y_j)\\ (y_{j+2}-y)^3-4(y_{j+1}-y)^3, & y\epsilon[y_j,y_{j+1})\\ (y_{j+2}-y)^3, & y\epsilon[y_{j+1},y_{j+2})\\ 0, & \text{otherwise}\end{cases} \quad (27)$$

ϑ_j with $j=0,1,2\ldots,N+1$ forms a basis in the $[a,b]$. At each node, the updated cubic B-spline functions are obtained as follows:

$$\psi_1(y)=\vartheta_1(y)+2\vartheta_0(y) \quad (28)$$

$$\psi_2(y)=\vartheta_2(y)-\vartheta_0(y) \quad (29)$$

$$\psi_j(y)=\vartheta_j, \quad \text{for} \quad j=3,\ldots.N-2 \quad (30)$$

$$\psi_{N-1}(y)=\vartheta_{N-1}(y)-\vartheta_{N+1}(y) \quad (31)$$

$$\psi_N(y)=\vartheta_N(y)+2\vartheta_{N+1}(y) \quad (32)$$

Here $\{\psi_1\psi_2,\ldots,\psi_N\}$ establishes a basis for said domain $[a,b]$. The coefficients a^*_{ij}, b^*_{ij} are computed by the updated cubic B-spline function. The estimation of first-order derivative is derived as:

$$\psi'_k(y_i)=\sum_{j=1}^{N} a^*_{ij}\vartheta_k(y_j) \quad \begin{matrix}\text{for} \quad i=1,2,\ldots,N\\ k=1,2,\ldots,N\end{matrix} \quad (33)$$

For the *first-knot* point y_1:

$$\psi'_k(y_1)=\sum_{j=1}^{N} a^*_{1j}\vartheta_k(y_j) \quad \begin{matrix}\text{for} \quad i=1,2,\ldots,N\\ k=1,2,\ldots,N\end{matrix} \quad (34)$$

Then system of equations is formed as:

$$\begin{bmatrix}6&1&0&0&&&&&\\0&4&1&0&\cdots&0&&0&\\0&1&4&1&&&&&\\ \vdots&&0&\ddots&0&&\vdots&&\\&&&&1&4&1&0\\0&&0&\cdots&0&1&4&0\\&&&&0&0&1&6\end{bmatrix}\times\begin{bmatrix}a^*_{11}\\a^*_{12}\\a^*_{13}\\\cdot\\\cdot\\\cdot\\a^*_{N-3}\\a^*_{N-2}\\a^*_{N-1}\\a^*_N\end{bmatrix}=\begin{bmatrix}-6/h\\6/h\\0\\\cdot\\\cdot\\\cdot\\0\\0\\0\\0\end{bmatrix} \quad (35)$$

Similarly, for the next node, y_2, we have:

$$\psi'_k(y_2)=\sum_{j=1}^{N} a^*_{2j}\vartheta_k(y_j) \quad \begin{matrix}\text{for} \quad i=1,2,\ldots,N\\ k=1,2,\ldots,N\end{matrix} \quad (36)$$

Then again, the system of equations is:

$$\begin{bmatrix}6&1&0&0&&&&&\\0&4&1&0&\cdots&0&&0&\\0&1&4&1&&&&&\\ \vdots&&0&\ddots&0&&\vdots&&\\&&&&1&4&1&0\\0&&0&\cdots&0&1&4&0\\&&&&0&0&1&6\end{bmatrix}$$

$$\times \begin{bmatrix} a^*_{21} \\ a^*_{22} \\ a^*_{23} \\ . \\ . \\ . \\ a^*_{2N-3} \\ a^*_{2N-2} \\ a^*_{2N-1} \\ a^*_{2N} \end{bmatrix} = \begin{bmatrix} -3/h \\ 0 \\ 3/h \\ 0 \\ . \\ . \\ 0 \\ 0 \\ 0 \\ 0 \end{bmatrix} \tag{37}$$

After for each y_i's, the system for the last node y_N is expressed as

$$\begin{bmatrix} 6 & 1 & 0 & 0 & & & & & \\ 0 & 4 & 1 & 0 & \cdots & 0 & & 0 & \\ 0 & 1 & 4 & 1 & & & & & \\ & \vdots & & 0 & \ddots & 0 & & \vdots & \\ & & & & & 1 & 4 & 1 & 0 \\ & 0 & & 0 & \cdots & 0 & 1 & 4 & 0 \\ & & & & & 0 & 0 & 1 & 6 \end{bmatrix}$$

$$\times \begin{bmatrix} a^*_{N1} \\ a^*_{N2} \\ a^*_{N3} \\ . \\ . \\ . \\ a^*_{NN-3} \\ a^*_{NN-2} \\ a^*_{NN-1} \\ a^*_{NN} \end{bmatrix} = \begin{bmatrix} 0 \\ 0 \\ 0 \\ 0 \\ . \\ . \\ 0 \\ 0 \\ -6/h \\ 6/h \end{bmatrix} \tag{38}$$

The solution of the above systems provides the coefficients, $a^*_{11}, a^*_{12} \ldots, a^*_{1N}$, $a^*_{21}, a^*_{22} \ldots, a^*_{2N} \ldots, a^*_{N1}, a^*_{N2} \ldots, a^*_{NN}$. Then the values of b^*_{ij} for $i = 1, 2, 3 \ldots N, j = 1, 2, 3 \ldots N$ are calculated as follows:

$$b^*_{ij} = \begin{cases} 2a^*_{ij}\left(a^*_{ij} - \dfrac{1}{y_i - y_j}\right) & \text{for} \quad i \neq j \\ -\sum\limits_{i=1, i\neq j}^{N} b^*_{ij} & i = j \end{cases} \tag{39}$$

The simplified system of differential equations is written as for $i = 1, 2, 3 \ldots, N$, as follows.

$$V_t = R(u_1, u_2, T_1, T_2, u_p, T_p) \tag{40}$$

We used the time-stepping system that is both robust and effective in maintaining stability Runge–Kutta (SSP-RK43) scheme[47] and[61] to solve this method in this paper:

$$V_1 = u_0 + \frac{\Delta t}{2} * R(u, u_2, T_1, T_2, u_p) \tag{41}$$

$$V_2 = u_1 + \frac{\Delta t}{2} * R(u_1, u_2, T_1, T_2, u_p, T_p) \tag{42}$$

$$V_3 = 2/3u_0 + \frac{u_1}{3} + \frac{\Delta t}{6} * R\left(u_1, u_2, T_1, T_2, u_p, T_p\right) \tag{43}$$

$$V_M = U_3 + \frac{\Delta t}{2} * R(u_1, u_2, T_1, T_2, u_p, T_p) \tag{44}$$

4. ENGINEERING DESIGN QUANTITIES

4.1. Skin Friction Coefficients

When the fluid flows over the channel walls (boundaries), it exerts a frictional effect on these surfaces, obstructing forward motion and causing skin friction (shear stress) on the surface. The *skin-friction coefficient* is used to quantify this effect. The expressions for *skin friction coefficients* at the lower and upper walls are defined as follows:

At lower wall

$$\left(C_f\right)_{y=-1} = \frac{2}{Re}\left[(1+\eta_1)\frac{\partial u_1}{\partial y} + \eta_1 M_1\right]_{y=-1} \tag{45}$$

At upper wall

$$\left(C_f\right)_{y=1} = \frac{2r_1}{r_2 Re}\left[(1+\eta_1)\frac{\partial u_1}{\partial y} + \eta_1 M_1\right]_{y=1} \tag{46}$$

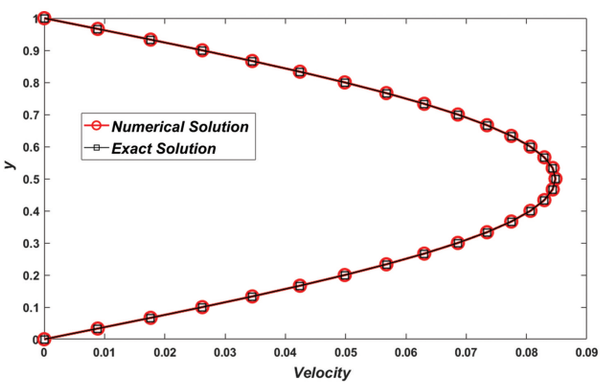

Fig. 2. Numerical versus exact solution.

ARTICLE

ARTICLE

4.2. Nusselt Numbers

Nusselt number is a key parameter in MHD nuclear and energy generator systems. It quantifies the rate of heat transfer from the bulk flow to the boundaries and also expresses the relative contribution of thermal convection heat transfer to thermal conduction heat transfer. The expressions for Nusselt number on both walls take the form:

At lower plate

$$(N_u)_{y=-1} = \left(-\frac{\partial T_1}{\partial y}\right)_{y=-1} \tag{47}$$

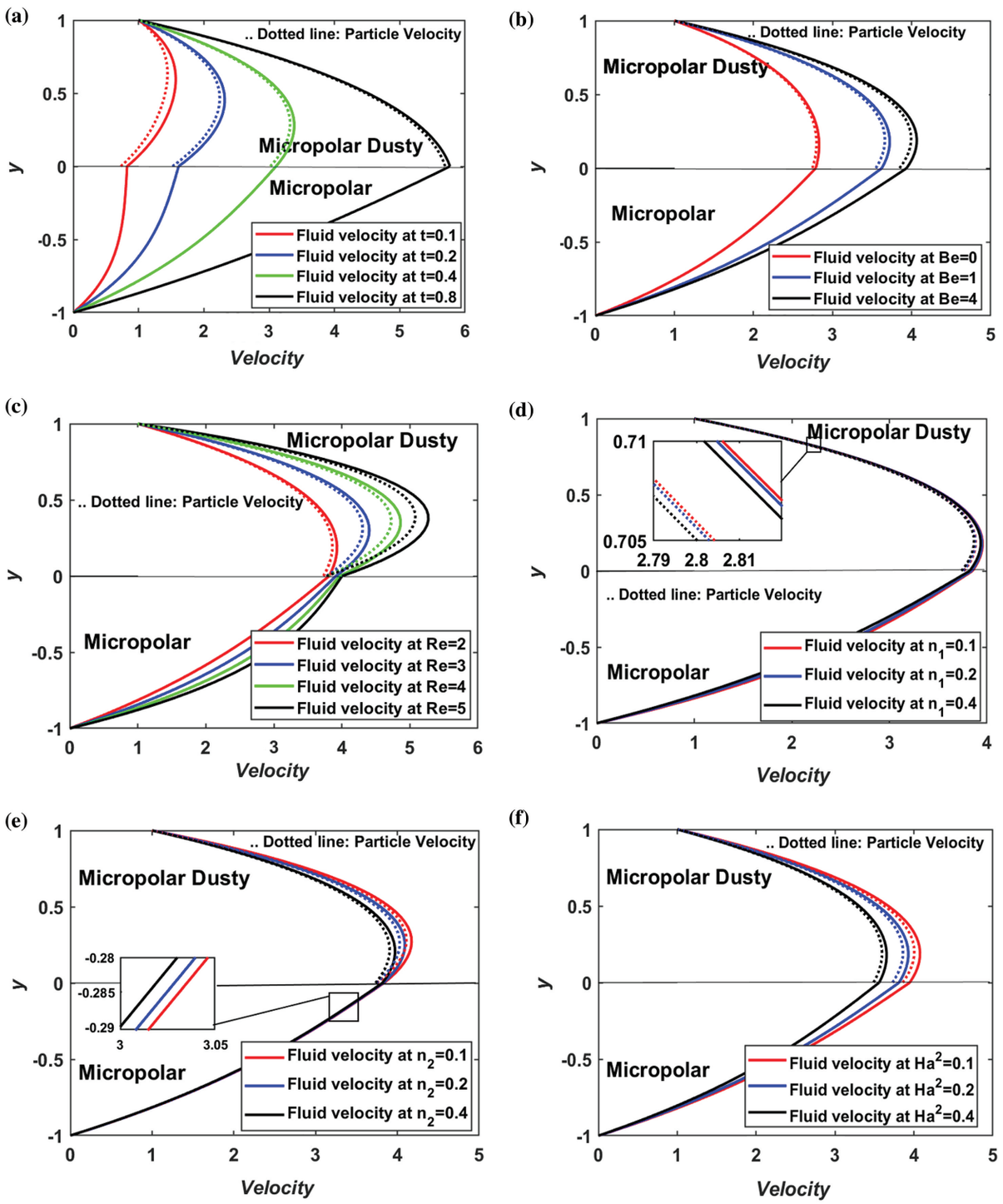

Fig. 3. Continued.

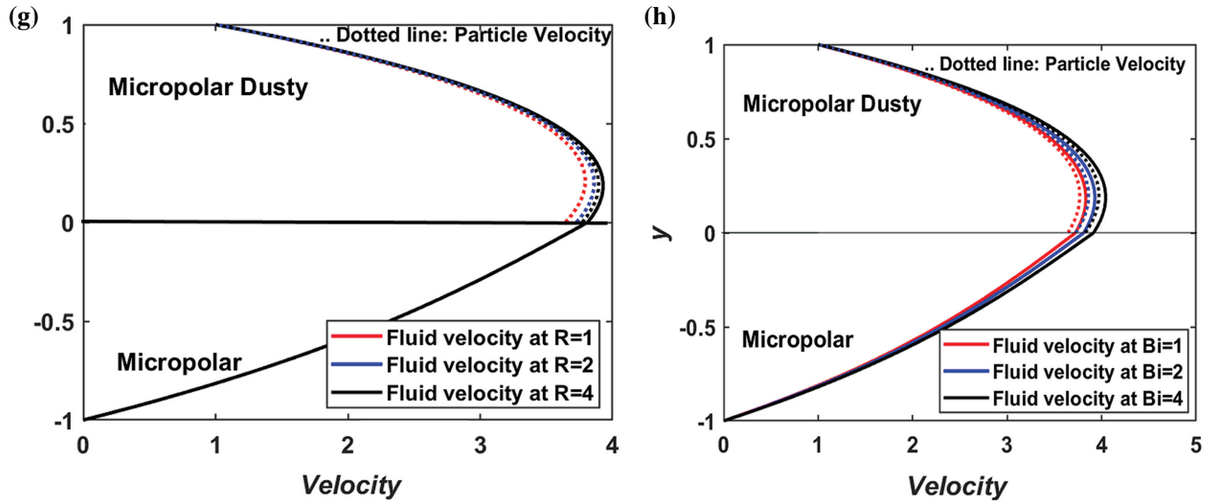

Fig. 3. Velocity profiles with varying parameters: (a) With time (b) with Hall parameter (c) with Reynolds number (d) with the lower fluid micropolar parameter (e) with the upper fluid micropolar parameter (f) with Hartmann number (g) with particle concentration parameter (h) with Ion-slip parameter.

At upper plate

$$(N_u)_{y=1} = \left(-\frac{\partial T_2}{\partial y}\right)_{y=1} \tag{48}$$

5. RESULTS AND DISCUSSION

The time-dependent unidirectional generalized hydromagnetic Couette flow of two immiscible, electro-conductive, dissipative, micropolar, and micropolar-dusty fluids with heat transfer has been examined theoretically. The two-fluid flow coupled problem (Eqs. (17)–(24)) in the corresponding regions with stable interface have been numerically solved by modified cubic B-spline differential quadrature method, and velocity, temperature profiles of fluids, and dust particles have been obtained. The analysis of skin friction coefficient and Nusselt number at both upper and lower boundaries of the duct have also been computed. The results are discussed in due course with the following prescribed values of all parameters (unless otherwise indicated): $Ge = 5,\ t = 0.5, \eta_1 = 0.5, \eta_2 = 0.5,\ Ha^2 = 2, Be = 2, Bi = 2,\ Re = 2, R = 2,\ r_1 = 0.5, r_2 = 0.5, r_3 = 100, C_r = 0.5, Ec = 0.5, Kr = 0.5, Pr = 2, \delta_1 = 2, \delta_2 = 2, Cr_r = 0.5$. This data represents real MHD generator duct flows and is consistent with relevant publications–see Refs. [35–38]. The simulation results are verified for the velocity profile by comparing them with the limiting case (the non-MHD, non-dusty, single Newtonian Couette flow for which $Ha^2 = 0, Be = 0, Bi = 0, R = 0, \eta_1 = 0, \eta_2 = 0, r_1 = 1, r_2 = 1 Ge = 0$). The limiting case numerical result and the exact solution (*Appendix*) shows strong agreement, as seen in Figure 2, and the parabolic laminar flow profile is captured across the channel span.

5.1. Analysis of Velocity Profiles

Figures 3(a)–(h) represents the effect of various fluid parameters on fluids and particle velocity and it is cited from Figures 3(a), (b), and (h) that both fluid and particle velocity increasing with time, Hall parameter ($Be = \sigma\beta B_0$) and Ion-slip parameter (Bi). The magnetic resistive force is decreased as Be and Bi are increased, creating an acceleration in the main flow, which increases fluid and particle-phase velocities. The Reynolds number $Re = (\rho_{1U_0 h})/\mu_1$ is the non-dimensional parameter which describes the ratio of inertial to viscous forces. Higher Re in the two-fluid medium indicates lower viscous forces. The viscous forces decrease as the Reynolds number increases, resulting in a growing pattern in fluid velocities (See Fig. 3(c)). Figures 3(d) and (e) show that increasing the micropolar parameters $\eta_1 = (\kappa_1/\mu_1)$ of micropolar fluid and $\eta_2 = (\kappa_2/\mu_2)$ of micropolar-dusty fluid (which increase the vortex viscosities κ_1 and κ_2) elevate the magnitudes of velocity profiles of the fluids and particle-phase increase in the respective regions. Therefore, increasing the spin of the microelements produces flow acceleration. Considering the fact that η_1 is a characteristic of micropolar fluid alone, it has a weaker effect on micropolar-dusty fluid as well; similarly η_2 is a feature of micropolar-dusty fluid alone and therefore has a less dramatic impact on micropolar fluid also. This happens due to the continuous coupling across the interface. The Hartmann number squared, $Ha^2 = (\sigma B_0^2 k^2)/\mu_1$ expresses the square of the ratio of the Lorentz magnetic drag force to the viscous hydrodynamic force. When Ha^2 is unity these two forces are balanced. When $Ha < 1$ magnetic drag exceeds viscous force and vice versa for $Ha > 1$. The influence of the transverse magnetic field on the hydromagnetic flow and thermal characteristics can be analyzed by changing this

number. According to Figure 3(f), increasing Ha^2 significantly elevates the magnetic retarding force and results in a depletion in the velocity fields in both regions. This may be attributed to the effect of an applied transverse magnetic field on both plates, which causes resistance to fluid movement through the Lorentz force, which substantially damps the flow. Figure 3(g) indicates that only the dust particle velocity increases with an enhancement of particle concentration parameter R, and no variation in fluid velocities is observed.

5.2. Analysis of Microrotation (Angular Velocity) Profiles

Figures 4(A)–(H) illustrates the effects of various fluid parameters on microrotations (angular velocities). It is observed from Figure 4(A), that the microrotation

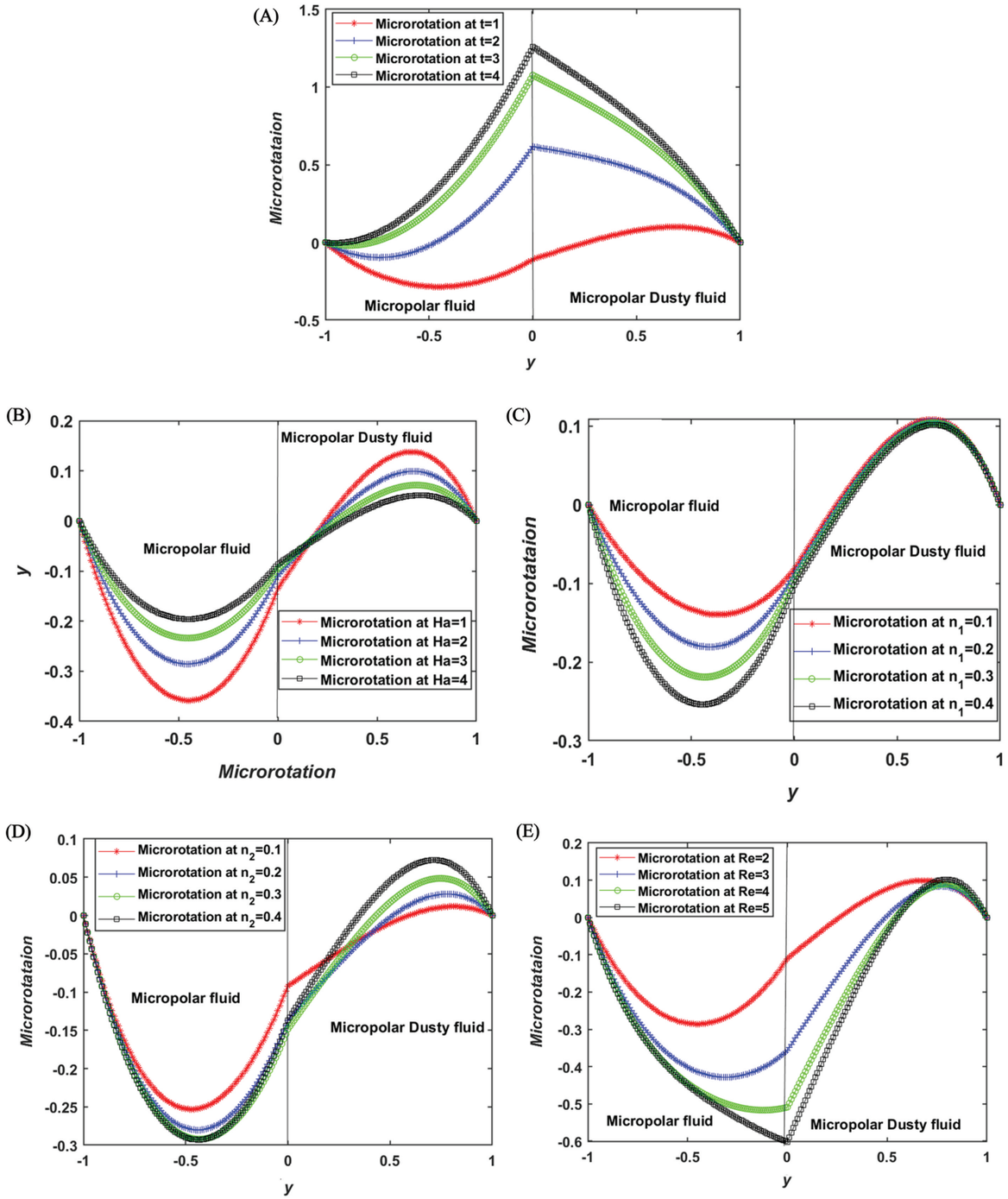

Fig. 4. Continued.

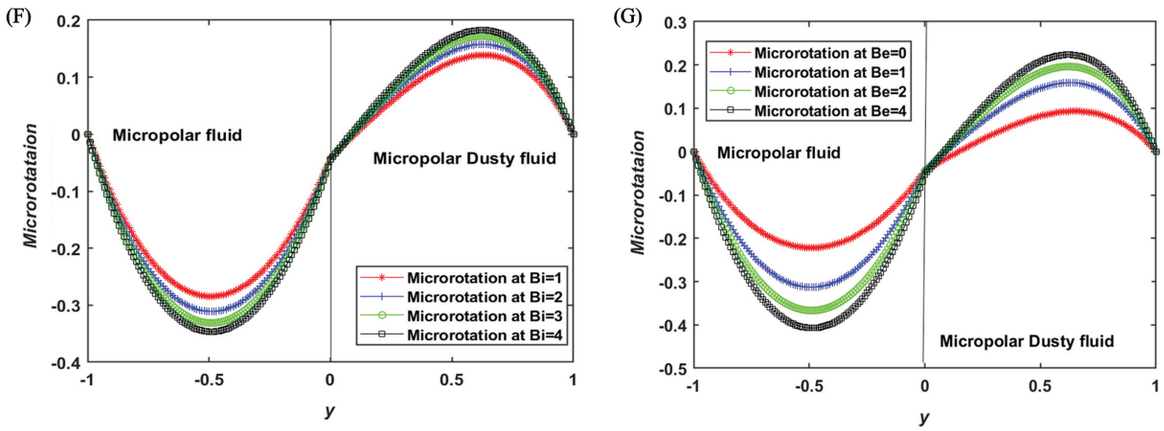

Fig. 4. Micropolar profiles with varying parameters: (A) With time (B) with Hartmann parameter (C) with the upper fluid micropolar parameter (D) with the lower fluid micropolar parameter (E) with Reynolds number (F) with Ion-slip parameter (G) with Hall parameter.

increases with time and attains a steady state after a significant time has elapsed. According to Figure 4(B), increasing Ha^2 manifests in a boost in microrotation in the *lower* region fluid; however, this response changes to a decrease in the *upper* region. Figure 4(C) shows that increasing micropolar parameter, η_1 of the micropolar fluid, decreases the microrotation profiles in both regions. However, a less marked decline is observed in the micropolar fluid region as compared to the micropolar dusty fluid region. Figures 4(D), (F), and (G) show that as the micropolar parameter of the micropolar dusty fluid η_2, Hall *parameter*(Be) and Ion-slip parameter (Bi) increase, microrotation consistently decreases in the *lower region* fluid (reduced spin of microelements) and the response is modified to an increasing nature in the upper region (i.e., faster spin of microelements). Figure 4(E) indicates that the microrotation profiles in both regions noticeably decrease with an increment in Reynolds number Re.

5.3. Analysis of Temperature Profiles

The nonlinear and flow-dependent viscous dissipation terms are also included in the numerical computations. Figures 5(I) to (XI) exhibit the effect of various fluid parameters on temperature profiles of micropolar and micropolar dusty fluids. It is evident from Figure 5(I), that the temperature profiles of both region fluids increase with progression in time. Elevation in the ratio of viscosity r_1 leads to an increase in the temperatures in both regions (see Fig. 5(II)). According to Figure 5(III), increasing Ha^2 (i.e., a boost in magnetic field strength) amplifies the impedance to the flow and increases temperatures. Figure 5(IV) shows that increasing Reynolds number Re reduces the viscous force hence temperature profiles of both fluids are increased. Figure 5(V) visualizes the effect of the *Eckert number*(Ec) on temperature evolution in the channeling regime. Ec provides a measure of kinetic energy dissipated via internal friction to the enthalpy difference across the channel. It is observed that the temperature of fluids and particle increase with Ec since greater mechanical energy is converted to heat which energizes the regime. It is noted from Figure 5(VI), that increasing the *Prandtl number* (Pr) i.e., ratio of viscous diffusivity to thermal diffusivity, enhances the temperature profiles of both fluids and particles. It can be seen from Figures 5(VII)–(X), that the temperature profiles of fluids and particles in both regions rise with an increment in the micropolar parameter of micropolar dusty fluid, η_2, Hall parameter (Be) and Ion-slip parameter (Bi). The temperature in both region fluids decreases with greater values of density ratio r_1 and micropolar parameter of the lower region fluid, η_1 (see Figs. 5(IX) and (XI)).

5.4. Analysis of Skin-Friction Coefficients

As the immiscible fluids flow internally over the boundaries of the channel, the maximum resistance to the flow is experienced. Since the only laminar flow is considered, the flow will not become chaotic at some point in the flow path, although Hartmann-Stokes layers will develop in the presence of a magnetic field. Frictional forces are applied to the boundary surface impeding flow- this is known as skin friction drag. Table I shows that skin friction increases with time *(t)*, Reynolds number (Re), Hall parameter (Be) and Ion-slip parameter (Bi) at the lower wall of the channel i.e. the flow is accelerated at the lower wall. However, a slight decrement is induced with an increment in the micropolar parameter of the lower zone fluid η_1, the micropolar parameter of the upper zone fluid η_2 and Hartmann number, Ha^2 but remains constant with increasing values of particle concertation parameter R. At the upper wall, a decrease in skin friction co-efficient is induced with rising values of time *(t)*, Reynolds number Re, Hall parameter (Be), and Ion-slip parameter (Bi). When η_1, η_2, and Ha^2 are increased, the skin co-efficient improves slightly but remains invariant with modification in particle concentration parameter R. It is important to note that mod-

ARTICLE

ern MHD generators are increasingly exploiting stronger magnetic fields with the advent of more powerful magnets. This amplifies the contribution of Hall currents and ion slip-neglecting these effects, therefore, leads to *under-prediction* in the skin friction coefficient at the lower wall and *over-prediction* at the upper wall. The Hall and ion slip effects will also modify the structure of the Hartmann-Stokes layers at the boundaries. The inclusion of Hall and ion slip current effects, therefore, provides for a more realistic appraisal of thermofluid characteristics in practical applications since the change in the magnitude and direction of the current density leads to a significant modification in Lorentz electromagnetic force, as noted by Kayukawa.[62]

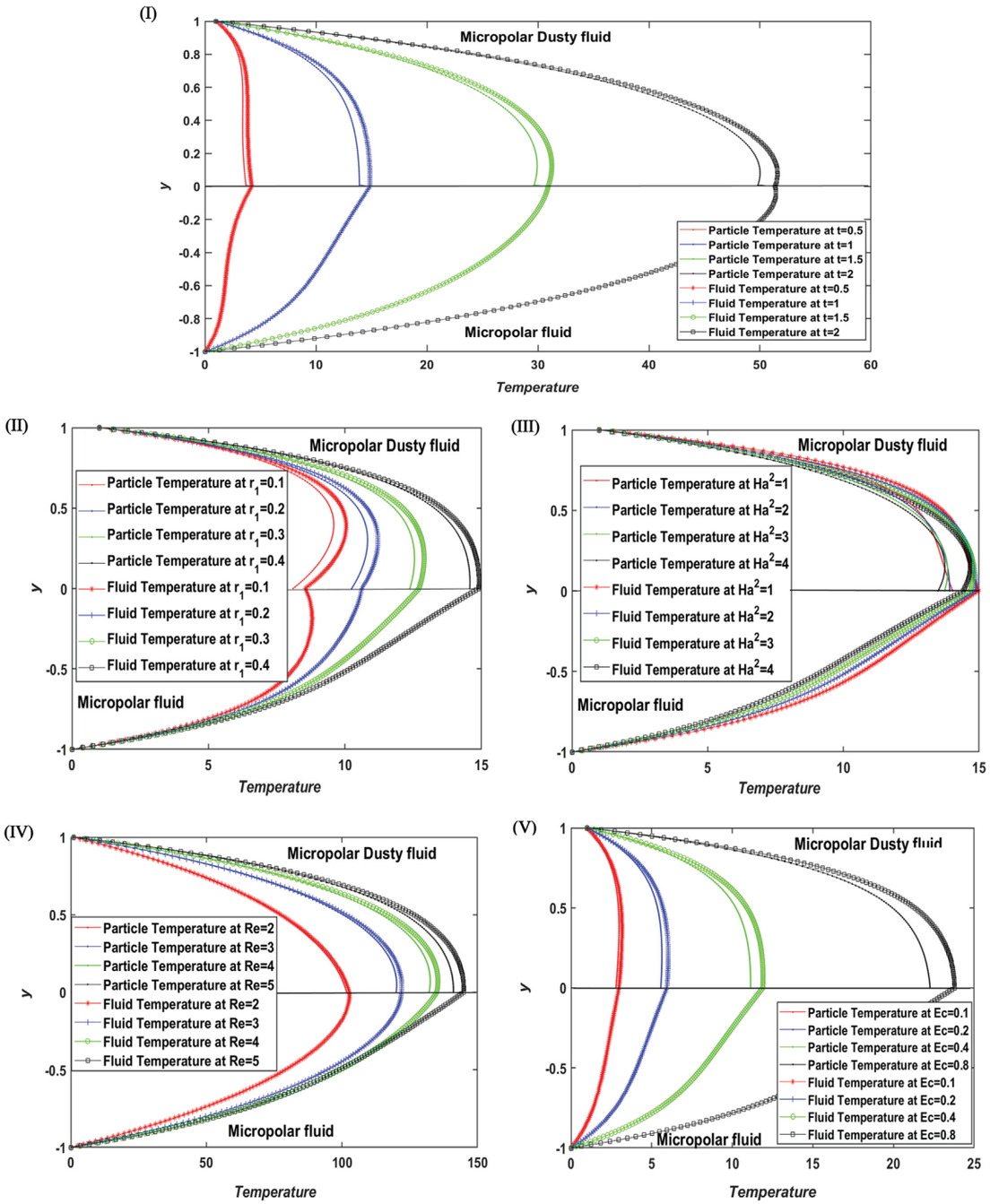

Fig. 5. Continued.

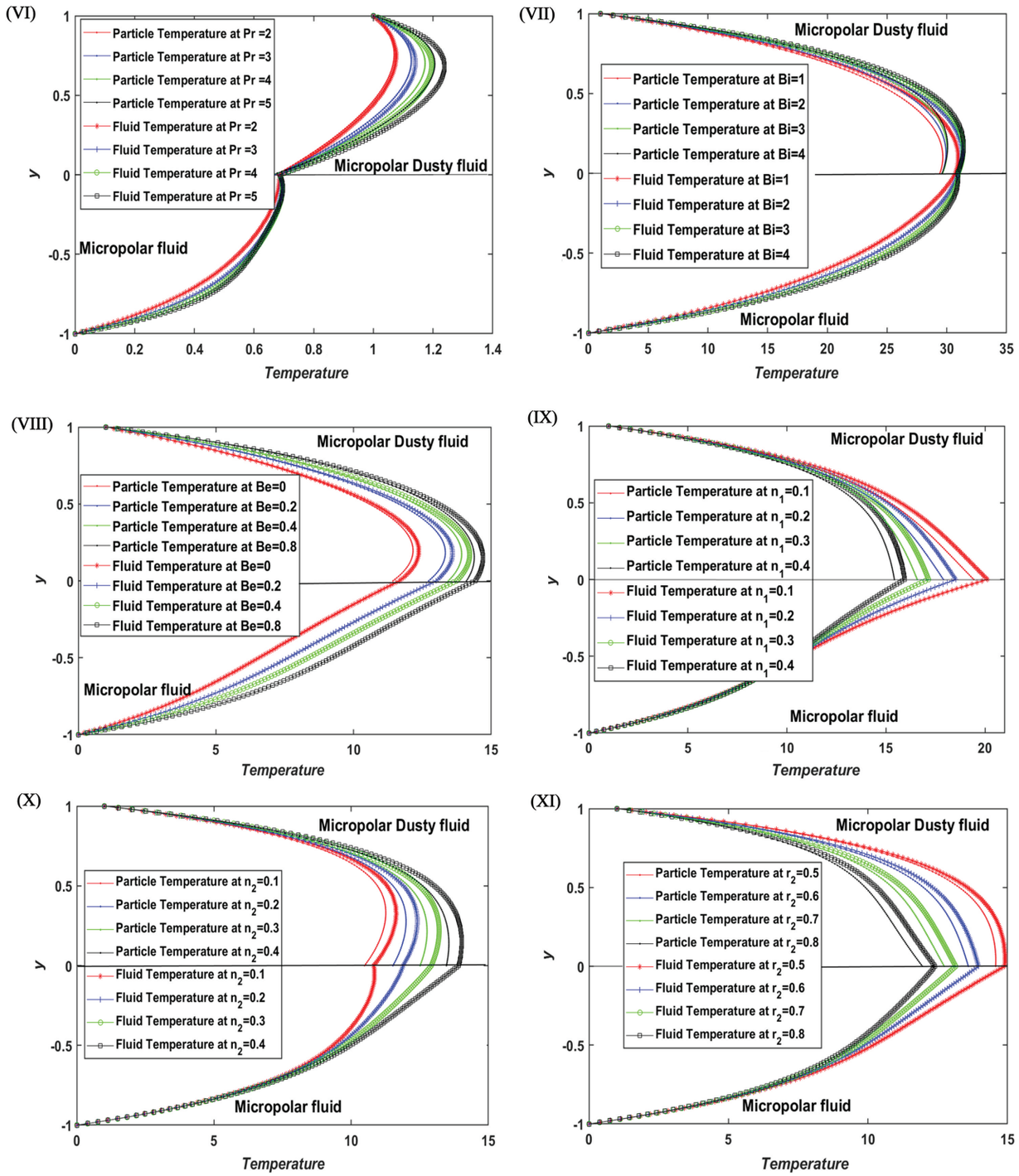

Fig. 5. Temperature profiles with varying parameters: (I) With time (II) with ratio of viscosity (III) with Hartmann number (IV) with Reynolds number (V) with Eckert number (VI) with Prandtl number (VII) with Ion-slip parameter (VIII) with hall parameter (IX) with the lower fluid micropolar parameter (X) with the upper fluid micropolar parameter (XI) with density ratio.

5.5. Analysis of the Nusselt Numbers

The Nusselt number, which is equal to the dimensionless temperature gradient at the wall also quantifies the ratio of convection heat transfer to conductive heat transfer at the surface. Table II shows that the Nusselt number increases at the upper wall and decrease at the lower wall with time (t), Reynolds number (Re), Eckert number (Ec), Prandtl number (Pr), Hall parameter (Be), Ion-slip parameter (Bi), the micropolar parameter of micropolar dusty fluid (η_2) and micropolar parameter of lower region fluid

Table I. Skin friction coefficient with varying parameters.

t	Lower Plt	Upper Plt	η_2	Lower Plt	Upper Plt	Be	Lower Plt	Upper Plt
0.1	3.914577	−5.03428	0.1	8.978459	−14.4407	0	7.175638	−7.88893
0.2	5.499268	−7.96846	0.2	8.955957	−13.6545	1	8.595216	−11.1443
0.4	7.853986	−10.8048	0.3	8.937793	−12.9805	2	8.911331	−11.8856
0.8	11.86768	−14.765	0.4	8.923136	−12.3965	4	9.119304	−12.3772
Re	Lower Plt	Upper Plt	Ha^2	Lower Plt	Upper Plt	R	Lower Plt	Upper Plt
2	8.911331	−11.8856	1	9.136863	−12.4189	1	8.911333	−11.8856
3	10.66685	−15.8778	2	8.911331	−11.8856	2	8.911331	−11.8856
4	12.26886	−19.5165	3	8.695507	−11.3788	3	8.91133	−11.8857
5	13.73152	−22.7994	4	8.488902	−10.8966	4	8.91133	−11.8857
η_1	Lower Plt	Upper Plt	Bi	Lower Plt	Upper Plt			
0.1	10.17517	−11.913	1	8.764204	−11.5398			
0.2	9.79548	−11.9073	2	8.911331	−11.8856			
0.3	9.464052	−11.9008	3	9.015624	−12.1318			
0.4	9.171692	−11.8936	4	9.084507	−12.2948			

Table II. Nusselt numbers at the upper and lower walls (plates = Plt) with various parameters.

t	Lower Plt	Upper Plt	Ha^2	Lower Plt	Upper Plt	Re	Lower Plt	Upper Plt	Kr	Lower Plt	Upper Plt
0.5	−10.6939	18.2945	1	−43.0247	57.7629	2	−39.6009	53.5489	0.1	−39.6009	159.8501
1	−39.6009	53.5489	2	−39.6009	53.5489	3	−41.1022	70.1412	0.2	−39.6009	99.94199
1.5	−82.8666	99.0824	3	−36.5677	49.8127	4	−42.4534	86.9392	0.4	−39.6009	62.20223
2	−132.946	147.186	4	−33.8719	46.489	5	−44.2968	104.621	0.8	−39.6009	39.63246
Ec	Lower Plt	Upper Plt	Pr	Lower Plt	Upper Plt	Bi	Lower Plt	Upper Plt	η_2	Lower Plt	Upper Plt
0.1	−7.92018	9.92662	2	−39.6009	53.54888	1	−37.5084	50.97172	0.1	−38.9077	48.0127
0.2	−15.8404	20.8322	3	−48.6417	70.42561	2	−39.6009	53.54888	0.2	−39.0412	49.3787
0.4	−31.6807	42.6433	4	−56.7456	85.78423	3	−41.1507	55.45682	0.3	−39.2043	50.7372
0.8	−63.3614	86.2656	5	−64.243	99.96635	4	−42.2057	56.75519	0.4	−39.3825	52.0479
Be	Lower Plt	Upper Plt	R	Lower Plt	Upper Plt	η_1	Lower Plt	Upper Plt			
0	−20.6741	30.16	1	−39.6004	53.57657	0.1	−36.8681	58.28132			
0.2	−25.4591	36.0918	2	−39.6009	53.54888	0.2	−37.5684	56.94946			
0.4	−29.0338	40.5148	3	−39.6011	53.53989	0.3	−38.2685	55.73181			
0.8	−33.6803	46.2526	4	−39.6013	53.53548	0.4	−38.95	54.60394			

(η_1). At the lower plate, the Nusselt number increases whereas it exhibits a decrement at the upper wall with an increment in Hartmann number squared, Ha^2. Nusselt number however remains constant at both channel walls with particle concertation parameter (R). The Nusselt number at the upper wall shows a decreasing nature with an increase in the thermal conductivity ratio k_r whereas it does not change at the lower wall.

6. CONCLUSIONS

A theoretical model of the transient magnetohydrodynamic flow of dual immiscible non-Newtonian micropolar and micropolar dusty fluids in a horizontal duct with heat transfer, viscous heating, Hall current, and ion slip effects has been developed. The robust modified cubic B-spline differential quadrature method (MCB-DQM) has been deployed to solve the transformed, dimensionless boundary value problem numerically. Extensive visualization of linear velocity, microrotation (angular velocity), and temperature profiles of both fluid and particle phases have been presented. Validation with exact solutions has also been included for the linear velocity field. A parametric study of the impact of all key thermophysical and electromagnetic parameters on thermofluidic characteristics has been conducted. The main conclusions of the current study are summarized as follows:

(i) For the regulating condition of non-dusty, single fluid Newtonian Couette flow, the modified cubic B-spline differential quadrature approach was found to be in good agreement with exact solutions.

(ii) Fluid velocities, microrotation (angular velocity), and temperature profiles of both fluids and particles are enhanced with time and for a higher time, the particle and fluid velocities are the same.

(iii) The *micropolar parameter* η_1 of lower region fluid influences the velocities and temperatures of upper region (micropolar dusty) fluid *and the impact of parameter* η_2 of the upper region, fluid is also being seen on lower region fluid velocities and temperatures.
(iv) The *Hall*(Be) and *Ion-slip*(Bi) parameters significantly increase the velocity and temperature of both fluids and the angular velocity of micropolar dusty fluid whereas they decrease the microrotation of micropolar fluid.
(v) *Hartmann number* (Ha^2) exhibits an inverse relationship with the velocities of the fluid and particle phases and their temperatures
(vi) *Reynolds number (Re)* affects the fluid and particle velocities and their temperatures with a directly proportional relation. However, *Re* shows an inverse relationship with the angular velocity.
(vii) Dust particle and fluid temperatures are both increased with an enhancement in *Eckert number* (Ec), the ratio of viscosities r_1 and *Prandtl number (Pr).*

Overall, the Modified cubic B-spline differential quadrature method (MCB-DQM) achieves excellent accuracy and is a very versatile method for addressing unsteady viscous multi-fluid non-Newtonian transport in MHD duct flows. The current work has provided a good benchmark for more general computational fluid dynamics simulations. However, it has neglected *magnetic induction effects* since it was assumed that the magnetic Reynolds number is sufficiently small to ignore the magnetic field distortion. Future work may include *induced* magnetic field phenomena in dusty flows from rotating disks (Von Karman swirl flows), pulsating plates, etc, including MHD and heat transfer especially electro and magneto micropolar rotating dusty flows and will be deported imminently.

APPENDIX

For non-magnetic, non-dusty, single fluid Newtonian Couette flow through the horizontal channel, the governing equation for momentum is simplified under appropriate initial and boundary conditions as:

$$\frac{\partial u}{\partial t} = \frac{1}{Re}\left[\frac{\partial^2 u}{\partial y^2}\right] \tag{49}$$

$$u(-1,t) = 0, \quad u(0,t) = 0 u(1,t) = 0,$$

$$u(y,0) = \sin \pi y; \tag{50}$$

The exact solution to the above problem is:

$$u = e^{-(\pi^2 t/Re)\cdot \sin \pi y} \tag{51}$$

NOMENCLATURE

$\varnothing$	Volume fraction function
σ	Electrical conductivity of fluids S/m
J	Current density Am^{-2}
B_0	Magnetic field A/m
Bi	Ion slip parameter
Be	Hall parameter
T_{w1}, T_{w2}	Temperatures of lower and upper plates K
U_0	The velocity of the upper plate m/s
u_1, u_2	Velocities of lower and upper region fluids m/s
u_p	Particle phase velocity m/s
M_1, M_2	Microrotations of lower and upper region fluids S^{-1}
T_1, T_2	Temperatures of lower and upper region fluids K
T_p	Particle phase temperature K
ρ_1, ρ_2	The density of lower and upper region fluids Kg/m^3
ρ_p	Particle density Kg/m^3
m_p	The average mass of particles kg
μ_1, μ_2	Viscosity co-efficient $kg \cdot m^{-1} \cdot s^{-1}$
κ_1, κ_2	Micropolar vortex viscosities
j_1, j_2	Gyration parameters
K_1, K_2	Thermal conductivities $W/m \cdot K$
C_{P1}, C_{P2}	Specific heat capacities $J \cdot kg^{-1} \cdot K^{-1}$
γ_1, β_1	Gyro-viscosity coefficients of lower region fluid
γ_2, β_2	Gyro-viscosity coefficients of upper region fluid
c_p	Specific heat capacity of the particles $J \cdot kg^{-1} \cdot K^{-1}$
K	Stokes drag coefficient
N	The number density of the dust particles m^{-3}
γ_T	Temperature relaxation parameter
Re	Reynolds number
η_1, η_2	Micropolar material parameters
Ha^2	Square of Hartmann magnetic number
Ec	Eckert number
Pr	Prandtl number
R	Particle concentration parameter
r_1	Ratio of viscosities
r_2	Ratio of densities
r_3	Particle and fluid density ratio
C_r	The ratio of specific heat capacities
K_r	The ratio of thermal conductivities
$C_{\Pr}$	Particle and fluid specific heat capacities ratio
p	Fluid pressure P
C_f	Skin friction coefficient
N_u	Nusselt number.

Ethical Compliance

This article does not contain any studies involving animals or humans performed by any of the authors.

Conflicts of Interest

The authors declare that they have no conflicts of interest.

Acknowledgments: The authors of this paper would like to pay sincere thanks to all the reviewers for giving valuable feedback to improve the manuscript. The authors declare that there is no funding source or any grant associated with this research article.

ARTICLE

ARTICLE

References and Notes

1. C. Eringen, Mechanics of Generalized Continua, *IUTAM Symposium* (**1968**), pp. 18–35.
2. C. Kang and A. Eringen, *Bull. Math. Biol.* 38, 135 (**1976**).
3. M. Fakour, A. Vahabzadeh, D. D. Ganji, and M. Hatami, *J. Mol. Liq.* 204, 198 (**2015**).
4. H. H. Sherief, M. S. Faltas, and S. El-Sapa, *Journal of Molecular Liquids* 290, 111165 (**2019**).
5. E. I. Saad and M. S. Faltas, *J. Mol. Liq.* 312, 113289 (**2020**).
6. S. A. M. Mehryan, M. Izadi, and M. A. Sheremet, *J. Mol. Liq.* 250, 353 (**2018**).
7. T. Javed and M. A. Siddiqui, *J. Mol. Liq.* 249, 831 (**2018**).
8. A. Tetbirt, M. N. Bouaziz, and M. Tahar Abbes, *J. Mol. Liq.* 216, 103 (**2016**).
9. Y. Menni, A. J. Chamkha, and A. Azzi, *Spec. Top. Rev. Porous Media* 9, 1 (**2019**).
10. M. Gnaneswara Reddy and M. Ferdows, *Journal of Thermal Analysis and Calorimetry* 143, 3699 (**2021**).
11. Y. Menni, A. J. Chamkha, and A. Azzi, *J. Appl. Comput. Mech.* 6, 741 (**2020**).
12. S. S. Ghadikolaei, K. Hosseinzadeh, M. Hatami, and D. D. Ganji, *J. Mol. Liq.* 268, 813 (**2018**).
13. S. S. Ghadikolaei, K. Hosseinzadeh, M. Yassari, H. Sadeghi, and D. D. Ganji, *J. Mol. Liq.* 244, 374 (**2017**).
14. S. S. Ghadikolaei, K. Hosseinzadeh, and D. D. Ganji, *Powder Technology* 338, 425 (**2018**).
15. H. Kaneez, M. Nawaz, and Y. Elmasry, *J. Therm. Anal. Calorim.* 1 (**2020**), DOI: 10.1007/s10973-020-10284-y.
16. H. A. Nabwey and A. Mahdy, *Results Phys.* 21, 103777 (**2021**).
17. S. Ahmad and S. Nadeem, *Int. J. Ambient Energy* 1 (**2020**), DOI: 10.1080/01430750.2020.1861090.
18. M. R. Eid and F. Mabood, *J. Therm. Anal. Calorim.* 143, 2419 (**2021**).
19. O. D. Makinde, K. G. Kumar, S. Manjunatha, and B. J. Gireesha, *Defect Diffus. Forum* 378, 125 (**2017**).
20. Y. Menni, A. Azzi, and A. Chamkha, *Journal of Thermal Analysis and Calorimetry* 135, 1951 (**2019**).
21. M. Devakar and T. K. V. Iyengar, *Eur. Phys. J. Plus* 128, 1 (**2013**).
22. M. Devakar and A. Raje, *Eur. Phys. J. Plus* 133, 1 (**2018**).
23. J. Srinivas and J. V. Ramana Murthy, *J. Eng. Thermophys* 25, 126 (**2016**).
24. J. Srinivas and J. V. Ramana Murthy, *Heat Mass Transf.* 6 (**2015**), DOI: 10.5098/hmt.6.4.
25. J. Srinivas and J. V. Ramana Murthy, *J. Appl. Mech. Tech. Phys.* 57, 997 (**2016**).
26. J. C. Umavathi, A. J. Chamkha, A. Mateen, and A. Al-Mudhaf, *Heat Mass Transf.* 42, 81 (**2005**).
27. J. C. Umavathi, J. Prathap Kumar, and A. J. Chamkha, *Turkish J. Eng. Environ. Sci.* 33, 221 (**2009**).
28. J. C. Umavathi, I. C. Liu, and M. Shekar, *Appl. Math. Mech.* 33, 931 (**2012**).
29. H. A. Attia, W. Abbas, and M. A. M. Abdeen, *J. Brazilian Soc. Mech. Sci. Eng.* 38, 2381 (**2016**).
30. H. A. Attia and K. M. Ewis, *Adv. Mech. Eng.* 11, 1 (**2019**).
31. M. Ashraf, N. Jameel, and K. Ali, *Appl. Math. Mech* 34, 1263 (**2013**).
32. M. Veera Krishna, M. Gangadhar Reddy, and A. J. Chamkha, *Int. J. Fluid Mech. Res.* 46, 1 (**2019**).
33. M. Veera Krishna, *Int. Commun. Heat Mass Transf.* 119, 104927 (**2020**).
34. M. V. Krishna, M. G. Reddy, and A. J. Chamkha, *J. Porous Media* 24 (**2021**), DOI: 10.1615/JPORMEDIA.2020025021.
35. K. V. Prasad, K. Vajravelu, P. S. Datti, and B. T. Raju, *J. Appl. Fluid Mech.* 6, 385 (**2013**).
36. M. Devakar and A. Raje, *J. Appl. Fluid Mech.* 12, 603 (**2019**).
37. M. V. Krishna and A. J. Chamkha, *Numer. Methods Partial Differ. Equ.* 37, 2150 (**2021**).
38. M. V. Krishna and A. J. Chamkha, *Int. Commun. Heat Mass Transf.* 113, 104494 (**2020**).
39. M. Veera Krishna and A. J. Chamkha, *Results Phys.* 15, 102652 (**2019**).
40. M. Veera Krishna, N. Ameer Ahamad, and A. J. Chamkha, *Ain Shams Eng. J.* (**2021**), DOI: 10.1016/j.asej.2020.10.028.
41. Y. Menni, A. J. Chamkha, A. Azzi, and C. Zidani, *Int. J. Fluid Mech. Res.* 47 (**2020**), DOI: 10.1615/InterJFluidMechRes.2019026753.
42. M. Veera Krishna, N. A. Ahamad, and A. J. Chamkha, *Ain Shams Eng. J.* 12, 2099 (**2020**).
43. Y. Menni, A. Azzi, and A. J. Chamkha, *Heat Transf. Res.* 50, 1781 (**2019**).
44. Y. Menni, A. J. Chamkha, N. Massarotti, H. Ameur, N. Kaid, and M. Bensafi, *Int. J. Numer. Methods Heat Fluid Flow* 30, 4349 (**2020**).
45. Y. Menni, A. Chamkha, C. Zidani, and B. Benyoucef, *Int. J. Numer. Methods Heat Fluid Flow* 30, 3027 (**2019**).
46. Y. Menni, A. Azzi, A. J. Chamkha, and S. Harmand, *Int. J. Numer. Methods Heat Fluid Flow* 29, 3908 (**2019**).
47. Y. Menni, A. Azzi, A. J. Chamkha, and S. Harmand, *J. Appl. Comput. Mech.* 5, 231 (**2019**).
48. G. Arora and V. Joshi, *Alexandria Eng. J.* 57, 1087 (**2018**).
49. K. Ramesh and V. Joshi, *Int. J. Comput. Methods Eng. Sci. Mech.* 20, 1 (**2019**).
50. R. Katta, R. K. Chandrawat, and V. Joshi, *Journal of Physics: Conference Series* 1531, 012090 (**2020**).
51. O. A. Bég, J. Zueco, and H. S. Takhar, *Communications in Nonlinear Science and Numerical Simulation* 14, 1082 (**2009**).
52. J. Zueco, O. A. Bég, and L. M. López-Ochoa, *Prog. Comput. Fluid Dyn.* 11, 116 (**2011**).
53. O. A. Bég, S. Abdul Gaffar, V. R. Prasad, and M. J. Uddin, *Eng. Sci. Technol. an Int. J.,* 19, 377 (**2016**).
54. S. R. Sheri, O. Anwar Bég, P. Modugula, and A. Kadir, *Comput. Therm. Sci.* 11 (**2019**), DOI: 10.1615/ComputThermalScien.2019026405.
55. A. Yamanishi, S. Ohmori, K. Tsuru, T. Tachiiri, H. Kusajima, and K. Momo, *Japanese Pharmacol. Ther.* 27, 33 (**1999**).
56. A. H. Eraslan, *AIAA J.* 7, 186 (**1969**).
57. O. A. Beg, M. Ferdows, M. E. Karim, M. M. Hasan, T. A. Bég, M. D. Shamshuddin, and A. Kadir, *Int. J. Appl. Comput. Math*. 6, 1 (**2020**).
58. O. Anwar Bég, T. A. Bég, M. Ferdows, V. Buddakkagari, A. Kadir, H. J. Leonard, and S. Kuharat, *Int. J. Appl. Electromagn. Mech.* 65, 371 (**2021**).
59. M. Nawaz and T. Zubair, *Results Phys.* 7, 4111 (**2017**).
60. Q. Wu, D. W. L. Schubring, and J. J. Sienicki, *Nucl. Eng. Des.* 237, 2114 (**2007**).
61. A. Korkmaz and I. Dat, *Eng. Comput. (Swansea, Wales)* 30, 320 (**2013**).
62. N. Kayukawa, *Progress in Energy and Combustion Science* 30, 33 (**2004**).